EFFECTS OF RAPID SPANWISE ROTATION ON TURBULENT CHANNEL FLOW WITH A PASSIVE SCALAR

Geert Brethouwer, Philipp Schlatter & Arne V. Johansson
Linné Flow Centre
KTH Mechanics
SE-100 44 Stockholm, Sweden

ABSTRACT

Direct numerical simulations of fully developed turbulent channel flow including a passive scalar rotating about the spanwise axis have been performed. The mean bulk Reynolds number, $Re_b = U_b h/\nu \geq 20000$, where U_b is the bulk mean velocity and h the channel half width, is higher than in previous simulations and the rotation rate covers a wide range. At moderate rotation rates, turbulence on the stable channel side is significantly less damped than in DNS at lower Re_b. At high rotation rates we observe re-occurring, quasi-periodic instabilities on the stable channel side. Between these events the turbulence is weak, but during the instability events the wall shear stress and turbulence intensity are much stronger. The instabilities are caused by structures resembling Tollmien-Schlichting (TS) waves that at some instant rapidly grow, then become unstable and finally break down into intense turbulence. After some time the TS waves form again and the process repeats itself in a periodic-like manner.

Mean scalar profiles are also strongly affected by rotation and large scalar fluctuations are found on the border of the stable and unstable channel side. The turbulent Prandtl/Schmidt number of the scalar is much less than unity if there is rotation. Predicting scalar transport in rotating channel flow will therefore pose a challenge to turbulence models.

INTRODUCTION

Rotating turbulent wall-bounded flows are found in many engineering applications. The rotation induces Coriolis forces often having a large influence on flow properties and as well as on mass and heat transfer. Brethouwer (2005) and others have shown through direct numerical simulations (DNS) and linear theory that spanwise rotation can damp as well as augment turbulence in a homogeneous shear flow depending on the sense and speed of rotation.

Plane channel flow with spanwise rotation has in particular been the subject of many studies. In this case the Coriolis force does not directly affect the mean flow, but it does affect turbulent Reynolds stresses and thereby indirectly affects the mean flow. Rotation has a different effect on the flow on the two sides of the channel since the ratios of the spanwise vorticity of the mean flow and the imposed rotation have opposite signs. This should result in asymmetric velocity and Reynolds stress profiles, which has indeed been confirmed by several studies. Johnston et al. (1972) carried out experiments at $Re_b = U_b h/\nu = 5750$ and $Ro_b = 2\Omega h/U_b \leqslant 0.21$, and $Re_b = 17500$ and $Ro_b \leqslant 0.081$. Here U_b is the bulk mean velocity, h the half-width of the channel, ν the viscosity and Ω the spanwise rotation speed. They observed a strong suppression of turbulence on the so-called stable side and the formation of large roll cells on the so-called unstable side of the channel if Ro_b is high enough. Other, more recent experiments by Nakabayashi and Kitoh (2005) at low Re_b and Ro_b showed a slight increase of the turbulence intensity on the unstable side and a strong turbulence damping on the stable side.

Numerical simulations of rotating channel flow are more numerous since the Coriolis are here relatively easy to include, in contrast to experiments. Kristoffersen and Andersson (1993), for example, performed DNS of spanwise rotating turbulent channel flow at $Re_\tau = u_\tau h/\nu = 194$, where u_τ is the friction velocity, and $Ro_b \leq 0.5$. The mean velocity profiles were asymmetric and approximately linear with a slope $\mathrm{d}U/\mathrm{d}y \simeq 2\Omega$ in the core region of the channel in their DNS, implying that the absolute mean vorticity is about zero. The Reynolds stresses on the stable side were increasingly reduced with rising Ro_b, while on the unstable side the wall-normal and spanwise stresses were significantly augmented by rotation. Like Johnston et al. (1972) they observed large longitudinal roll cells for $Ro_b \geq 0.1$, but in their DNS at $Ro_b = 0.15$ the roll cells were persistent whereas in the experiments they appeared highly unsteady.

Recently, Grundestam et al. (2008) performed DNS of spanwise rotating channel flow at $Re_\tau = 180$ and a wide range of rotation speeds with Ro_b up to 2.49, i.e., significantly higher than in the previous studies. They found evidence for large streamwise vortices which were unsteady in space and time in a DNS at $Ro_b = 1.27$. Turbulence was strongly damped and the flow became laminar-like at high Ro_b on the stable channel side. At even higher Ro_b they found that the turbulence was also suppressed on the unstable side. The Reynolds shear stresses were then small everywhere and, as a result, the mean flow approached the laminar parabolic profile. Wallin et al. (2011) studied this case further and showed through inviscid linear stability analysis that all cross flow modes are damped for $Ro_b \geq 3.0$. If viscous effects are included all cross flow modes are damped at some critical Ro_b

slightly below 3.0. The analysis was confirmed by fully nonlinear DNS showing that above this critical Ro_b an initially fully turbulent flow relaminarizes. This means that linear effects are dominating at high Ro_b.

Since rotation affects turbulence it will also influence heat transfer rates and mixing of scalars. DNS of homogeneous shear flow (Brethouwer 2005), and DNS of spanwise rotating channel flow at $Re_\tau = 150$ (Nagano and Hattori 2003) and $Re_\tau = 194$ (Liu and Lu 2007) showed indeed a large effect of rotation on both the rate and direction of passive scalar transport. However, in the channel flow DNS Ro_b was moderate.

The objective of this study is to examine effects of spanwise rotation on turbulent channel flow with a passive scalar through DNS at higher Reynolds numbers than in previous studies and for a wide range of rotation speeds. In particular, we aim to study the effect of the Reynolds number on flow laminarization and the effect of high rotation speeds on passive scalar transport. Further, we want to generate data for validation of Reynolds averaged Navier Stokes (RANS) and scalar transfer models, and subgrid-scale (SGS) models for large-eddy simulations. This is strongly needed since modelling rotating turbulent flows including heat and mass transfer remains a challenge. Previous DNS data at low Reynolds numbers are arguably less useful for validating turbulence models for engineering applications, where Reynolds numbers are commonly much higher, and for validating SGS models due to the limited range of scales.

DIRECT NUMERICAL SIMULATIONS

We have performed DNS of fully developed spanwise rotating channel flow with a passive scalar. The DNS code uses Fourier expansions in the homogeneous directions and Chebyshev polynomials in the wall-normal direction. The passive scalar value is fixed at 0 at one wall and at 1 at the other, and its Prandtl number is 0.71. The domain size is $8\pi h \times 3\pi h$ in the streamwise and spanwise direction in all cases, larger than in most previous DNS of rotating channel flow, and the spatial resolution in terms of wall units is similar as in other well-resolved DNS. In all simulations the flow rate was kept constant. The parameters of the DNS are listed in table 1.

Table 1. DNS parameters: N_x, N_y and N_z are the number of modes in the streamwise, wall-normal and spanwise direction respectively. Re^u_τ and Re^s_τ are based on the friction velocity on the unstable, u^u_τ, and stable side, u^s_τ, of the channel respectively. Re_τ is based on $u_\tau = (u^{u2}_\tau/2 + u^{s2}_\tau/2)^{1/2}$.

Ro_b	Re_b	Re_τ	Re^u_τ	Re^s_τ	$N_x \times N_y \times N_z$
0	20000	1000	1000	1000	$2560 \times 385 \times 1920$
0.15	20000	975	1108	821	$2304 \times 385 \times 1728$
0.45	20000	800	963	595	$2048 \times 361 \times 1536$
0.9	20000	550	679	379	$1536 \times 257 \times 1152$
1.2	20000	426	503	331	$1152 \times 217 \times 864$
1.5	30000	414	461	361	$1024 \times 193 \times 768$
2.1	30000	315	316	314	$864 \times 193 \times 640$
2.4	30000	303	306	299	$640 \times 193 \times 512$

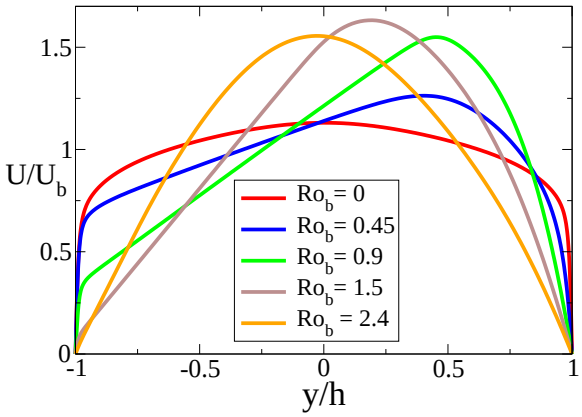

Figure 1. Mean flow profiles scaled with U_b at different Ro_b.

RESULTS

In this section we present the results of the DNS. Although the statistics are not yet fully converged in all runs, they nonetheless reveal some clear trends. The flow statistics of the run without rotation at $Re_\tau = 1000$ agree very well with the channel flow data by del Álamo et al. (2004) at $Re_\tau = 934$, the slight differences can be attributed to Reynolds number effects.

Velocity field

Figure 1 shows mean streamwise velocity profiles scaled with U_b of five runs with and without rotation. The runs at $Ro_b = 0.45$, 0.9 and 1.5 show the typical asymmetric velocity profile that is linear with $dU/dy \simeq 2\Omega$ in the core region of the channel implying that the sum of the mean flow and system rotation is zero. This has also been observed in the previous simulations of rotating channel flow, see e.g. Grundestam et al. (2008). At $Ro_b = 2.4$ the profile approaches the parabolic velocity profile of a laminar flow, indicating that the turbulent Reynolds stresses are very weak.

Figure 2 shows the friction velocities u^u_τ and u^s_τ on the unstable and stable channel side respectively scaled with $u_\tau = (u^{u2}_\tau/2 + u^{s2}_\tau/2)^{1/2}$ for all runs and including the DNS data of Kristoffersen and Andersson (1993), and Grundestam et al. (2008). The difference in the friction velocities at both wall first grows due to the augmention and damping of turbulence on the unstable and stable side respectively, but then it declines as Ro_b increases. At very high Ro_b, u^u_τ and u^s_τ should be equal since the flow is laminar in that case and the profile symmetric. In our DNS, the maximum difference in the friction velocities at the two walls is larger and occurs at a higher Ro_b than in DNS at lower Re_τ. Table 1 shows that Re_τ goes down at a fixed Re_b if Ro_b increases. At $Ro_b \geq 2.1$, Re_τ approaches 300, which is the friction Reynolds number of a

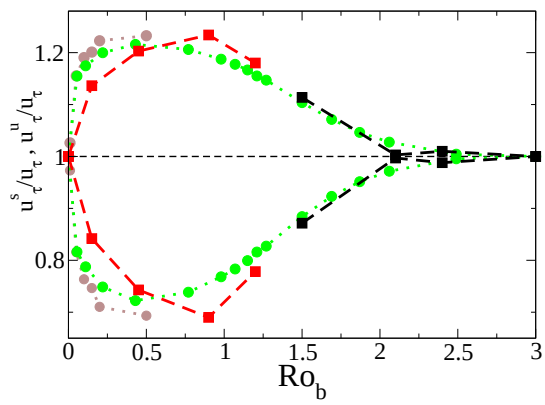

Figure 2. The normalized friction velocity on the unstable side, u_τ^u/u_τ, and on the stable side, u_τ^s/u_τ as function of Ro_b. Red squares and dashed lines, our DNS at $Re_b = 20000$; Black squares and dashed lines, our DNS at $Re_b = 30000$; Green circles and dotted lines, DNS of Grundestam et al. (2008) at $Re_\tau = 180$; brown circles and dotted lines, DNS by Kristoffersen and Andersson (1993) at $Re_\tau = 194$.

laminar flow at $Re_b = 30000$, hence the flow is apparently almost laminar.

Root-mean-square (rms) values of the streamwise, u^+, and wall-normal velocity fluctuations, v^+, scaled with u_τ are shown in figure 3. We see that the near-wall peak of u^+ on the unstable channel side first slightly goes up but then declines when Ro_b rises whereas on the stable side the peak rapidly disappears. At $Ro_b = 2.4$ the streamwise fluctuations are very weak in the whole channel. The wall-normal fluctuations change even more drastically. We see that v^+ strongly goes up on the unstable channel side when Ro_b rises and only at very high rotation speeds starts to decline, whereas on the stable side v^+ rapidly declines. At $Ro_b = 1.5$ and 2.4 there is a large region where the wall-normal fluctuations are very small indicating that the flow is almost laminar on the stable side. DNS data of Grundestam et al. (2008) at $Ro_b = 0.43$ are also included in figure 3 and can be compared to our DNS data at $Ro_b = 0.45$ and $Re_\tau = 800$. In particular the velocity fluctuations on the stable side are much more intense in our DNS, indicating that influence of the Reynolds number on the relaminarization is large.

Figure 4 shows the production of turbulent kinetic energy in terms of wall units $\mathscr{P}^+$ on the unstable and stable side. At $Ro_b = 0$ the peak value of $\mathscr{P}^+$ is close the limit 0.25 for nonrotating channel flow. The peak of $\mathscr{P}^+$ on the unstable side increases significantly up to Ro_b, showing the destabilizing effect of rotation, and then declines. On the stable side $\mathscr{P}^+$ rapidly declines with increasing Ro_b and the production of turbulent kinetic energy becomes very small and almost negligible at high Ro_b. For $Ro_b \geq 0.9$ we can in fact observe a region where $\mathscr{P}^+$ is negative, meaning that the turbulence transfers kinetic energy to the mean flow. Johnston et al. (1972) also claimed that they observed extended regions with negative production on the stable side when relaminarization occurred in their rotating channel flow experiments.

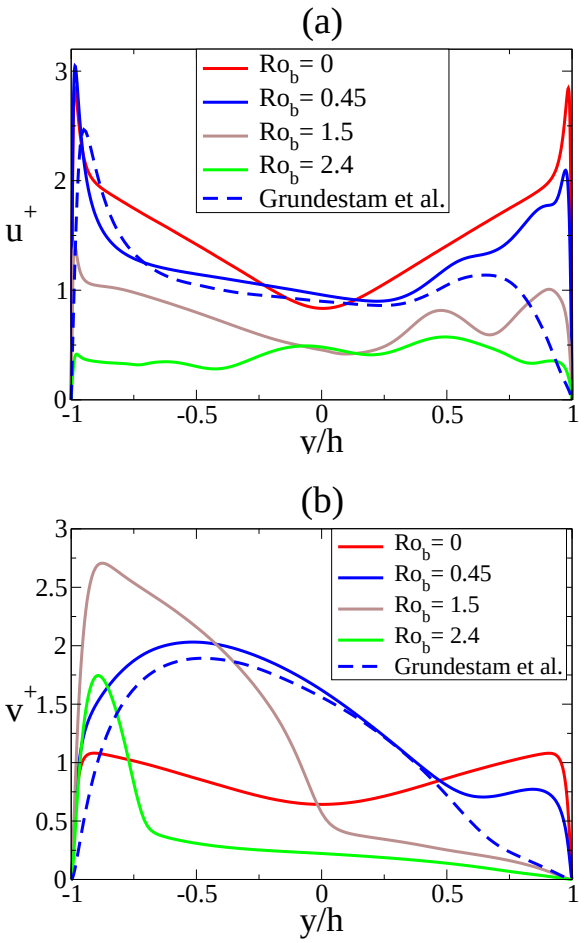

Figure 3. (a) u^+ and (b) v^+ at different Ro_b. DNS data of Grundestam et al. (2008) at $Ro_b = 0.43$ (blue dashed line) are also included.

Scalar field

Mean scalar profiles and the root-mean-square of the scalar fluctuations are shown in figure 5. The fluctuations are scaled with scalar wall-units Q_w/u_τ. Here, Q_w is the mean scalar flux at the wall which should be equal on both walls when the scalar field is in equilibrium. The mean scalar gradient away from the wall rapidly declines on the unstable channel side when Ro_b rises and is much smaller than on the stable side implying that turbulent scalar fluxes are much larger on the unstable side. Besides a near-wall peak on the unstable side, the scalar fluctuation profiles have a large peak on the border of the unstable and stable side where the mean scalar gradient abruptly and drastically increases in the rotating cases. Particularly, at $Ro_b = 0.9$ the scalar fluctuations are here very intense. In addition, the profiles have also a near-wall peak on the stable side. This differs from the results of DNS at lower Re_τ which showed only two maxima, one on the unstable and one on the stable side (Nagano and Hattori 2003, Liu and Lu 2007).

Profiles of the normalized mean streamwise and wall-normal fluxes are shown in figure 6. Away from the wall, the streamwise turbulent scalar flux sharply declines with increasing Ro_b and almost disappears on the unstable side. The nor-

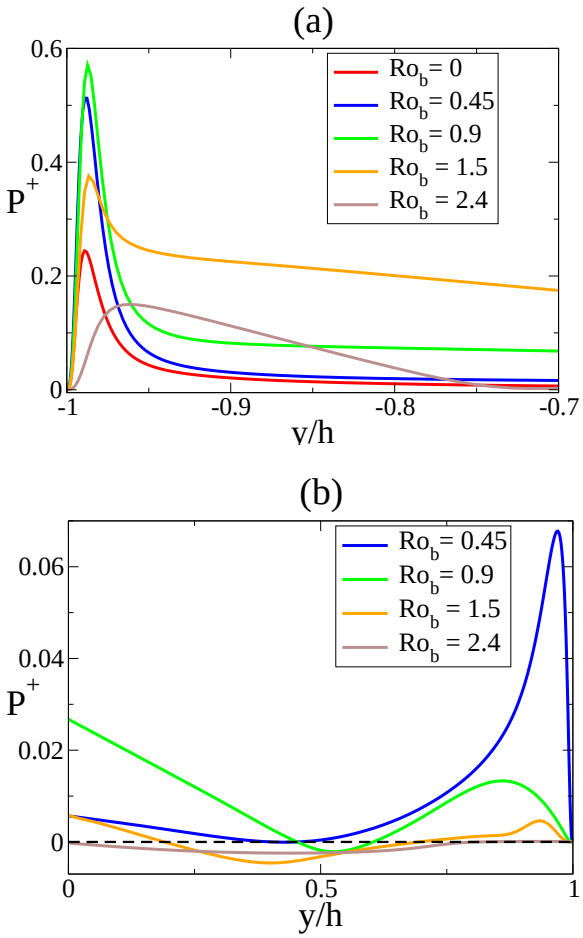

Figure 4. $\mathscr{P}^+$ on the unstable side (a) and stable side (b) in terms of wall units.

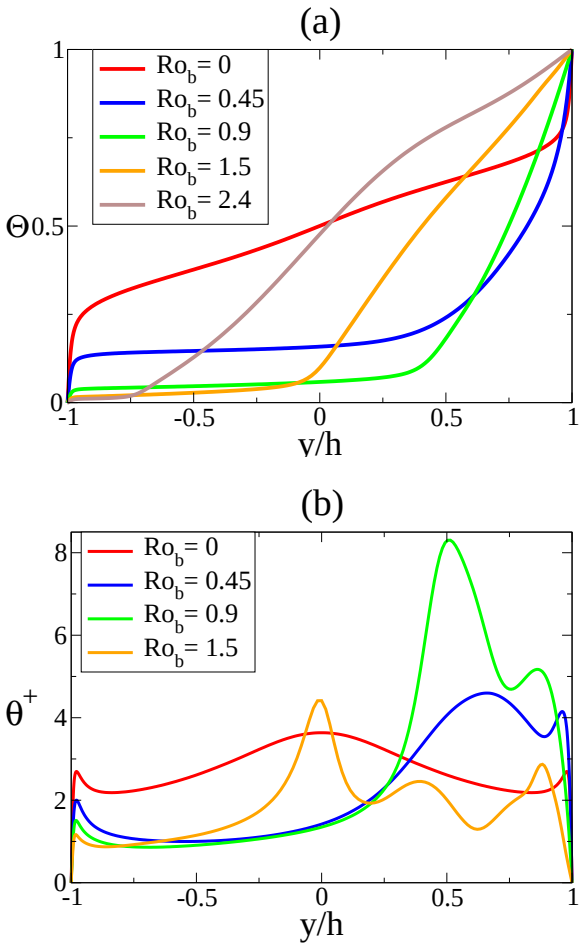

Figure 5. (a) Mean scalar and scalar fluctuations profiles (b) at different Ro_b.

malized wall-normal scalar flux is approximately equal to one on the unstable side and thus the scalar transport is predominantly turbulent, whereas it decreases with increasing Ro_b on the stable side. At $Ro_b = 1.5$ there is a significant region where the turbulent mean wall-normal scalar flux is negligible, hence the scalar transport is mostly molecular.

Figure 7 shows the Nusselt number $Nu = 2Q_w h/\kappa\Delta\Theta$, where κ is the scalar diffusivity and $\Delta\Theta$ is the difference of the imposed scalar value on the two walls. In our case, Nu is exactly the ratio of the mean scalar wall flux in the turbulent and laminar cases. At low to moderate Ro_b turbulence is very effective at enhancing scalar transport, but Nu rapidly declines with increasing Ro_b and approaches one, meaning that rotation strongly inhibits turbulent transport of the scalar.

Figure 8 shows the computed turbulent Prandtl Pr_T number of the scalar on the unstable channel side. At $Ro_b = 0$ it is close to unity, similar as in previous studies of scalar or heat transport in turbulent shear flows, but Pr_T strongly declines when Ro_b rises signifying relatively high scalar eddy diffusivities. Already at $Ro_b = 0.15$ it is much less than unity away from the wall. These results make clear that the commonly used eddy diffusivity models are not suitable for predicting heat and mass transfer in rotating wall-bounded flows, therefore more advanced models, like the explicit algebraic scalar models developed by Younis et al. (2010) which can incorporate rotation effects, are needed in such cases.

Quasi-periodic instabilities

At high rotation speeds we observed intense bursting events in our simulations which have not been reported before for fully developed rotating turbulent channel flow. The strong intermittency is, for example, seen in long times series of wall shear stresses τ_w and rms value of the streamwise velocity fluctuations u_{rms} integrated over the whole domain at $Ro_b = 1.2$ and $Ro_b = 1.5$ shown in figure 9. The wall shear stress on the unstable side exhibits little variations, but the time series of τ_w on the stable side and u_{rms} show both sharp, quasi-periodic increases in both runs. We observed qualitatively similar behaviour in time series in all runs with $Ro_b \geq 0.9$.

Figure 10 shows the statistics of the velocity fluctuations during the calm periods in between the bursting events and at the moment when a burst occurs at $Ro_b = 1.2$. We can observe that the fluctuations on the unstable side are hardly affected by the bursts. However, the velocity fluctuations, especially in the streamwise and spanwise direction, are very intense on the stable side during the bursting events, while in the calm

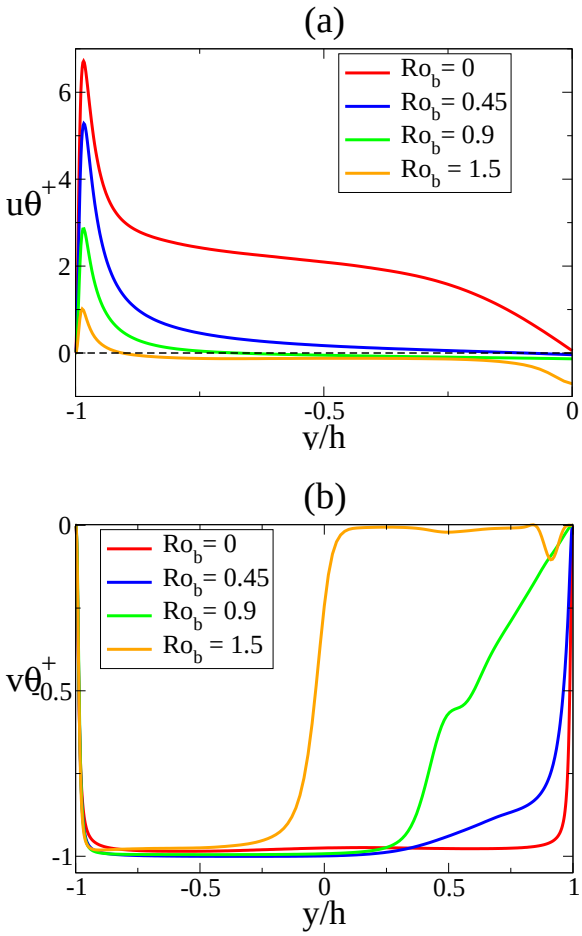

Figure 6. (a) Mean streamwise and (b) wall-normal turbulent scalar flux profiles in wall-units.

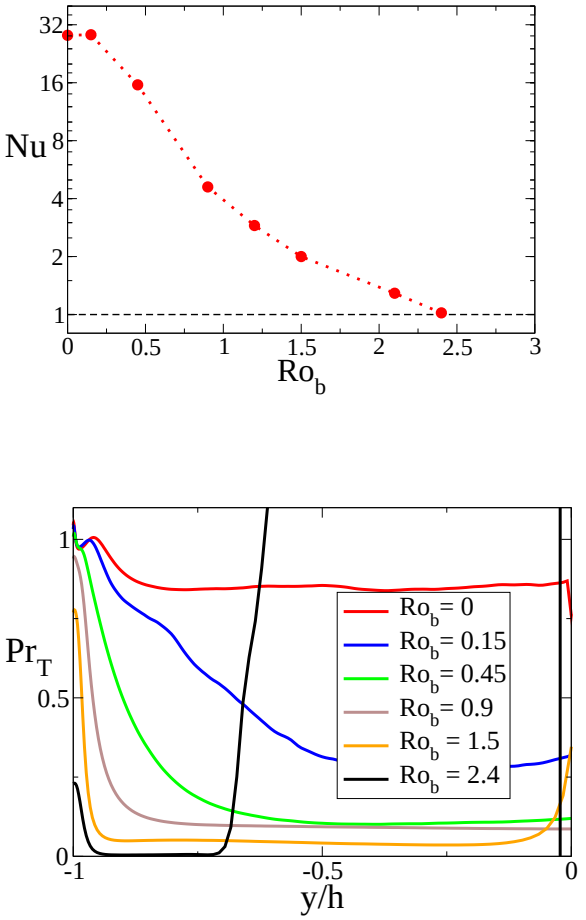

Figure 8. Turbulent Prandtl number on the unstable side at different Ro_b.

periods the fluctuations are weak. The bursting events therefore appear to be mostly confined to the stable channel side.

Visualizations give an indication of the cause of the periodic-like instabilities. Figure 11, for example, shows snapshots of the wall-normal velocity in the $x-y$ plane and streamwise velocity in the $x-z$ plane close to the wall on the stable side at $Ro_b = 1.2$. These snapshots have been taken some time before an intense bursts occurs. We observe clear, almost two-dimensional waves with a wave vector in the streamwise direction which resemble Tollmien-Schlichting (TS) waves. The wave length of these large structures seems to vary with Ro_b but is in this particular run about $2\pi h$. These waves can only be seen on the stable side, the other side is intensely turbulent.

According to linear stability analysis by Wallin et al. (2011) rotation damps all modes at high rotation rates, except the modes with spanwise wave number equal to zero, i.e. the waves that we observe in the snapshots. Usually, the formation of two-dimensional TS waves is inhibited by turbulence in wall-bounded flows. The hypothesis is that in spanwise rotating channel flow TS waves can develop since the turbulence is weak on the stable side. At some instant, the amplitude of the waves grow very rapidly. Visualizations as in figure 12 show that the waves become unstable and Λ-shaped vortices form, presumably due to nonlinear mechanisms. Thereafter, the waves break down completely into intense turbulence. The turbulence then decays since it is damped by the rotation. After some time the two-dimensional waves can develop again when the turbulence is sufficiently weak and the whole cycle repeats itself resulting in the quasi-periodic bursting events. Wallin et al. (2011) observed those instabilities also in rotating channel flow DNS at $Re_\tau = 180$ at very high rotation speeds. Our simulations show that the instabilities can also occur at higher Re_τ and at lower rotation speeds, as low as $Ro_b = 0.9$, when the flow on the unstable side is strongly turbulent.

We would like to acknowledge the computation time provided by PDC, the Swedish National Infrastructure for Computing and the Knut and Alice Wallenberg (KAW) Foundation. The project was supported by the Swedish Research Council through grant nr. 621-2010-4147.

REFERENCES

del Álamo, J. C., Jiménez, J., Zandonade, P., and Moser, R. D., 2004, "Scaling of the energy spectra of turbulent chan-

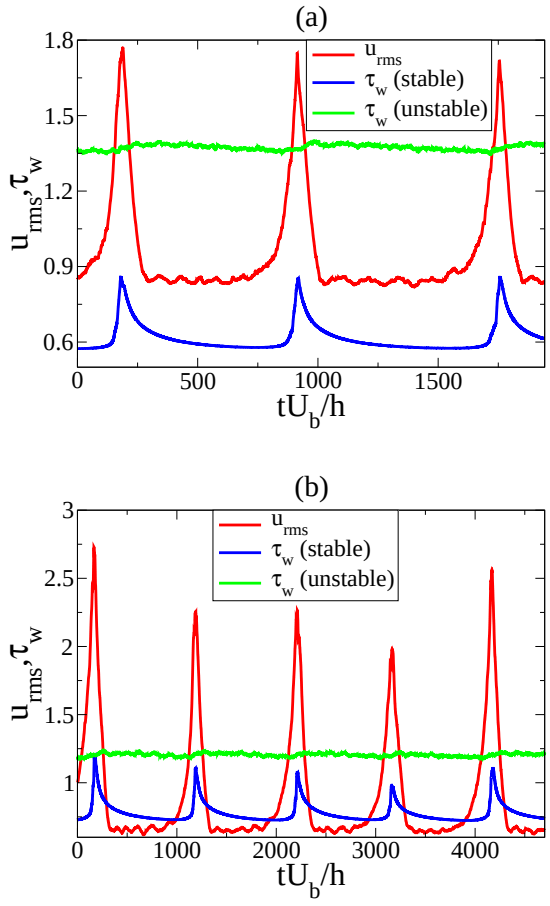

Figure 9. Times series of the wall averaged τ_w on the unstable and stable side and the volume integrated rms of the streamwise velocity fluctuations at (a) $Ro_b = 1.2$ and (b) $Ro_b = 1.5$.

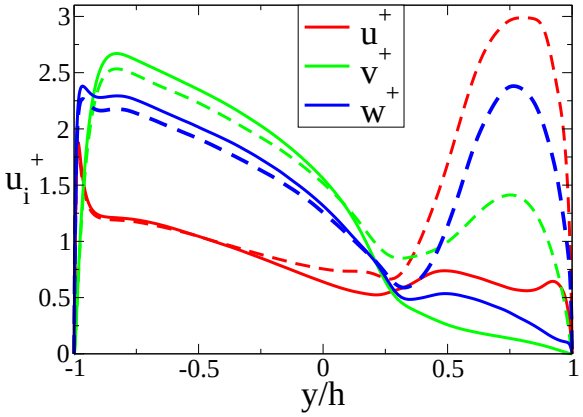

Figure 10. Rms velocity fluctuation profiles of all three components during the calm periods (solid lines) and bursts (dashed lines) at $Ro_b = 1.2$.

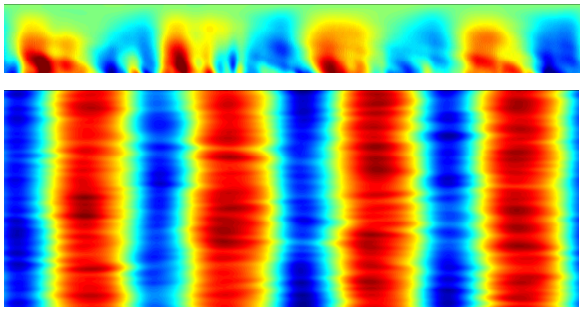

Figure 11. Snapshots of the wall-normal fluctuations in the $x-y$ plane and streamwise velocity fluctuations in the $x-z$ plane on the stable side at $Ro_b = 1.2$.

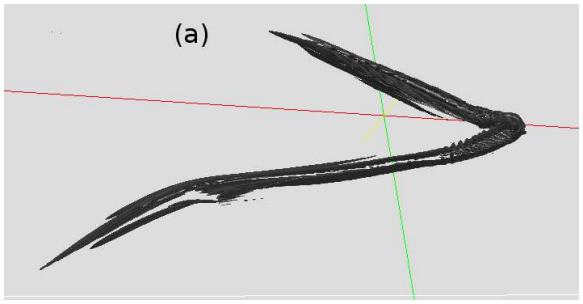

Figure 12. λ_2 visualization of a Λ-shaped vortex on the stable side at $Ro_b = 1.2$.

nels", *J. Fluid Mech.* **500**, 135–144.

Brethouwer, G., 2005, "The effect of rotation on rapidly sheared homogeneous turbulence and passive scalar transport. Linear theory and direct numerical simulations", *J. Fluid Mech.* **542**, 305–342.

Grundestam, O., Wallin, S., and Johansson, A. V., 2008, "Direct numerical simulations of rotating turbulent channel flow", *J. Fluid Mech.* **598**, 177–199.

Johnston, J. P., Halleen, R. M., and Lezius, D. K., 1972, "Effects of spanwise rotation on the structure of two-dimensional fully developed turbulent channel flow", *J. Fluid Mech.* **56**, 533–557.

Kristoffersen, R., and Andersson, H. I., 1993, "Direct simulations of low-Reynolds-number turbulent flow in a rotating channel", *J. Fluid Mech.* **256**, 163–197.

Liu, N.-S., and Lu, X.-Y., 2007, "Direct numerical simulation of spanwise rotating channel flow with heat transfer", *Int. J. Numer. Methods Fluids* **53**, 1689–1706.

Nagano, Y., and Hattori, H., 2003, "Direct numerical simulation and modelling of spanwise rotating channel flow with heat transfer", *J. Turbulence* **4**, 010.

acteristics of two-dimensional channel flow with system rotation", *J. Fluid Mech.* **528**, 355–377.

Younis, B. A., Weigand, B., Mohr, F., and Schmidt, M., 2010, "Modeling the effects of system rotation on the turbulent scalar fluxes", *J. Heat Transfer* **132**, 051703.

Wallin, S., Grundestam, O., and Johansson, A. V., 2011, "Laminarization mechanisms in rapidly rotating plane channel flow", *Submitted for publication*.